arXiv:1205.6161v1 [cond-mat.quant-gas] 28 May 2012

Scattering and absorption of ultracold atoms by nanotubes

B. Jetter[1], J. Märkle[1], P. Schneeweiss[1,2], M. Gierling[1], S. Scheel[3], A. Günther[1], J. Fortágh[1], and T. E. Judd[1]
[1] *CQ Center for Collective Quantum Phenomena and their Applications in LISA+,*
Physikalisches Institut, Eberhard-Karls-Universität Tübingen,
Auf der Morgenstelle 14, D-72076 Tübingen, Germany
[2] *TU Wien, Atominstitut, Stadionallee 2, 1020 Wien, Austria and*
[3] *Institut für Physik, Universität Rostock, Universitätsplatz 3, D-18051 Rostock, Germany*
(Dated: March 5, 2013)

We study cold atoms scattering from static and vibrating nanotubes. We find the scattering potential calculations for dielectric tubes can be greatly simplified with a modified pairwise summation approach. Quantum reflection of atoms from a nanotube is shown to become important if a Bose-Einstein condensate is used. Non-trivial absorption of atoms by nanotubes, as seen in experiments, is explained by inter-atomic interactions and quantum pressure. Natural nanotube vibrations do not significantly reduce condensate fractions, but lower frequency oscillations can dramatically heat the cloud.

PACS numbers: 34.20.-b, 34.50.Cx, 61.48.De, 67.85.-d

Interfacing ultracold atom clouds with micro- and nanoscaled objects enables exciting possibilities for creating hybrid quantum systems which combine the long quantum coherence times of ultracold atoms with the flexibility of other molecular, optical and solid state technologies [1–3]. There has been work on cold atoms with ions and superconductors [4–6], proposals for hybrid nanosystems [7–9] and recent experiments in which the interaction between cold atoms and carbon nanotubes was observed and measured [10, 11].

However, there is much to learn about how atoms scatter from nanostructures, or are absorbed by them. This is because theories of dispersion forces only become simple in very basic geometries where the finite size of the objects is neglected; this often cannot be done in the case of nanosystems. In addition, scattering of ultracold atoms is expected to take place in the crossover region between the non-retarded and retarded zones of the potential, which complicates the theory further. Recent experiments with ultracold atoms and carbon nanotubes raised further questions regarding the applicability of classical scattering theories [12], non-dynamical approaches [4], the role of quantum reflection and the effect of vibrations in the nanotubes. Better understanding of the dispersion interactions and scattering in such systems is crucial to future hybrid experiments and will aid the design of nanotechnologies where such forces exert a profound influence on their mechanical properties. It may also provide insight into the manufacture of nanostructures since this is often done from the vapor phase.

In this paper, we study how cold atoms are either elastically scattered from, or absorbed by, a nanotube. We begin by calculating the Casimir-Polder potentials for conducting and insulating tubes and then use these potentials to study the likelihood of elastic scattering by considering quantum reflection probabilities. We then perform dynamical simulations of a Bose-Einstein condensate (BEC) interacting with a nanotube to determine the rate at which atoms are lost due to inelastic scattering. Finally, we consider how an oscillating nanotube can affect the condensate fraction of a cold atom cloud when the two are overlapped, again by performing time-dependent simulations.

The interaction between an atom and a cylindrical, electrically neutral solid object is expected to be dominated by dispersion forces, specifically the Casimir-Polder (CP) potential. This subject has been considered by several groups [13–18] and is complicated by the fact that the properties of the cylinder alter not only the strength coefficients, but also the functional form of the potential [13].

The potential in the case of an atom and an infinitely long tube can be calculated using the general Lifshitz formula [19–21]

$$V_{CP}(r) = \mu_0 k_B T \sum_{l=0}^{\infty}{}' \xi_l^2 \alpha(i\xi_l) \mathrm{Tr}\left[\mathbf{G}^{(s)}(r,r,i\xi_l)\right] \qquad (1)$$

where $r = \sqrt{x^2+y^2}$ is the separation between the atom (in the x-y plane) and the tube axis z, T is the temperature of the tube, $\xi_l = 2\pi k_B T l/\hbar$ are the imaginary Matsubara frequencies with mode number l (the dash on the sum implies half weight for the first term), $\alpha(i\xi_l)$ is the polarizability of the atom, and the trace is taken over $\mathbf{G}^{(s)}(r,r,i\xi_l)$, the scattering part of the Green's polarizability tensor for the tube.

Equation (1) is appropriate for conducting and insulating tubes, but the potential in the insulating case can be approximately modeled by using the simpler pairwise summation approach, which is used for AFM tips and nanostructures [22] and is efficient for arbitrary geometries. The interaction energy can then be expressed as

$$V_{CP}(r) = -\int_V \frac{C(r,\xi)}{r_{pws}^6}\, dx\, dy\, dz \qquad (2)$$

where r_{pws} is the separation between the atom and a

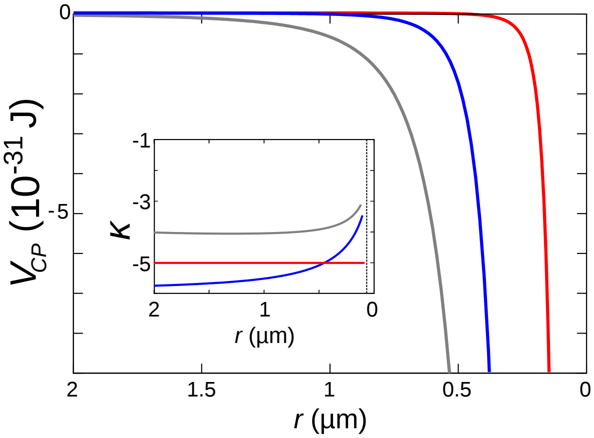

FIG. 1: (a) CP potential energy curves for a nanotube. Conducting tube, Liftshitz model (gray curve), dielectric tube, pairwise summation model (blue curve) and the $-C_5/r^5$ potential (red curve). Inset: effective power law, κ, for the three cases, color scheme as in the main plot. The dotted line marks the position of the tube surface.

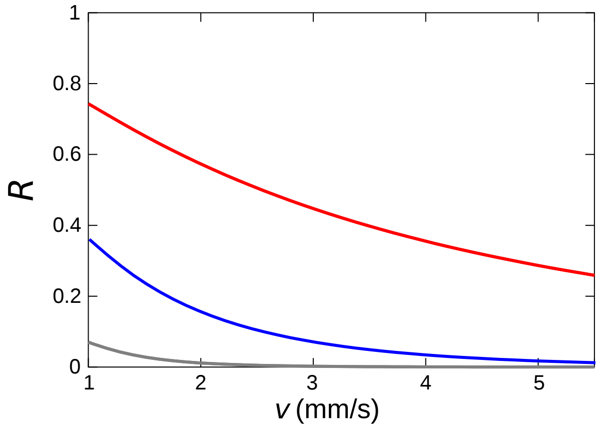

FIG. 2: Quantum reflection probabilities, R, from the different nanotube potential models. Conducting tube (gray curve), dielectric tube (blue curve) and the $-C_5/r^5$ potential (red curve).

discrete piece of the tube, $C(r,\xi)$ is the strength coefficient, and the integral takes place over the volume of the tube, V. C may be calculated as a function of r and ξ to provide approximate corrections due to retardation and temperature effects. We use [19]

$$C(r,\xi) = 6k_BT \sum_{l=0}^{\infty}{}' \frac{\alpha(i\xi_l)\beta(i\xi_l)}{(4\pi\epsilon_0)^2} \times \left(1 + r_l + \frac{5}{12}r_l^2 + \frac{1}{12}r_l^3 + \frac{1}{48}r_l^4\right) e^{-r_l} \qquad (3)$$

where $r_l = (2\xi_l/c)r_{pws}$ with c the vacuum speed of light. $\beta(i\xi_l)$ is the polarizability of a discrete piece of nanotube used for the pairwise summation. As $\alpha(i\xi)$ generally decays much more rapidly with frequency than $\beta(i\xi)$, we can use static tube polarizabilities to a good approximation. Finally, we consider the simplest approximation $V_{CP}(r) = -C_5/r^5$ which is a limit of the pairwise approach, assuming $L \gg r \gg R_0$ in the non-retarded regime, where R_0 is the radius of the tube.

We plot the potential for ^{87}Rb atoms interacting with a nanotube at $T = 300\,K$ in Fig. 1 assuming $R_0 = 63.5\,\text{nm}$ [11]. The ^{87}Rb polarizability is taken from [23]. We plot one curve (gray) using Eq. (1) and the Green's tensor from [21], which is for a good conductor. The blue curve is plotted using Eqs. (2) and (3) with a tube length $L = 10\,\mu$m and β calculated assuming a dielectric constant $\epsilon = 2.5$. The red curve is plotted using the $-C_5/r^5$ model with $C_5 = 6 \times 10^{-65}\,\text{J m}^5$, as obtained in recent experiments [10]. We see that the potential becomes strong on ultracold atomic energy scales ($\sim 10^{-31}$ J) about $0.5\,\mu$m from the surface. The conducting tube generally delivers the strongest potential, as expected. The $-C_5/r^5$ potential is around three orders of magnitude weaker. We calculated the potential for a dielectric cylinder using the Green's tensor approach [24] but have not plotted it here since it is barely distinguishable from the pairwise summation curve, the difference being $\sim 5\%$. This is significant since Eq. (2) can typically be calculated orders of magnitude faster than Eq. (1) and is immediately extendable to arbitrary geometries. It is, however, crucial that retardation corrections are included using Eq. (3).

The inset of Fig. 1 shows the effective power laws for the curves, $\kappa = d(\log V_{CP})/d(\log r)$, plotted against r. The gray curve (conducting tube) goes to $\kappa = -3$ at the surface and tends to $\kappa \approx -4$ with increasing r. By contrast, the dielectric model (blue curve) is closer to $\kappa = -5$, indicated by the red line.

We now analyze quantum reflection of atoms from the tube. For simplicity, we restrict our analysis to the perpendicular component of incident k-vectors, k_{perp} and reduce to problem to one dimension (1D). The quantum reflection probabilities can then be calculated with 1D Schrödinger wavepackets in a harmonic trap [25]. The condition for strong quantum reflection is given by $\Phi(k) = (1/k^2)dk/dr \sim d\lambda_{dB}/dr \gtrsim 1$ [26] where the local wave number, $k = 2\pi/\lambda_{dB}$, depends on the de Broglie wavelength, λ_{dB}, for the atom's center-of-mass motion. This defines a quantum reflection zone, which typically lies between $r \sim 60\,\text{nm}$ and $r \sim 2\,\mu$m for cold atoms. Atoms which come closer than the inner boundary cannot reflect and are absorbed by the nanotube. We model this effect with an imaginary potential [27]. The reflection probabilities, R, for the three different potentials are plotted in Fig. 2 for perpendicular incident velocities in the range $v_{perp} = \hbar k_{perp}/m = 1 \cdots 5\,\text{mm}\,\text{s}^{-1}$ which are common to ultracold atom clouds. We see that the conducting tube (gray curve) barely reflects ^{87}Rb atoms at the relevant ultracold velocities, which is expected for stronger potentials [28]. The insulating tube reflects atoms better but only delivers probabilities above ~ 0.2 when the velocities drop below $\sim 2\,\mathrm{mm\,s^{-1}}$. This corresponds to a thermal cloud with $T \sim 40\,\mathrm{nK}$. The $-C_5/r^5$ potential delivers noticeably higher reflection probabilities but they are still $\ll 1$ for clouds with $T > 100\,\mathrm{nK}$, mean speed $> 5\,\mathrm{mm\,s^{-1}}$. We note that quantum reflection is higher for the nanotubes than would be expected for planar surfaces [25] since the potentials are steeper and better fulfill the quantum reflection condition.

The results suggest that quantum reflection is likely to play an important role if a BEC is made to interact with a nanotube. A stationary BEC has no center-of-mass motion, but the curvature of the wavefunction can create a quantum pressure on an absorbing surface, which leads to atom loss, and hence, atom flow with velocities on the order of $\lesssim 1\,\mathrm{mm\,s^{-1}}$ [25]. We now investigate the interaction of a ^{87}Rb BEC with a nanotube. We use the simple $-C_5/r^5$ potential and assume a cylindrical symmetry with the tube fully overlapped in the center of the BEC. We model the dynamics of the condensate using the Gross-Pitaevskii equation (GPE)

$$-\frac{\hbar^2}{2m}\nabla^2\Psi + V_E\Psi + \frac{4\pi\hbar^2 a}{m}\left|\Psi\right|^2\Psi = i\hbar\frac{\partial\Psi}{\partial t} \qquad (4)$$

where $a = 5.4\,\mathrm{nm}$ is the s-wave scattering length, ∇^2 is the Laplacian in cylindrical coordinates, and $\Psi(z,r,t)$ is the wave function at time t, normalized such that $|\Psi|^2$ is the number of atoms per unit volume. The external potential, V_E, is a combination of the $-C_5/r^5$ potential and the harmonic trap. As with the reflection simulations, we employ imaginary potentials to absorb atoms that do not reflect. We choose $\omega_z = 2\pi \times 80\,\mathrm{rads\,s^{-1}}$ and $\omega_r = 2\pi \times 37\,\mathrm{rads\,s^{-1}}$ in the vertical and horizontal (radial) directions respectively, which are close to recent experiments [10]. The initial atom number is chosen by averaging the first two points of the experimental curve we wish to compare with. Spin flip losses are expected to be negligible [21].

We plot the atom number against time in Fig. 3 for the simulation (blue curve) and the corresponding experimental loss curve (black points). The loss curve is non-trivial showing a wide range of loss rates but the agreement with experiment is good. Atoms are accelerated towards the tube and the slow initial loss rate increases as atoms are rapidly removed from the BEC. This generates collective oscillations in the trap, shown in the inset of Fig. 3, along with sounds waves and phase gradients that can produce interference patterns. The subsequent fast loss rate flattens into a plateau; at this point very few atoms are near the trap center due to the in-trap oscillations. Finally for $t \gtrsim 0.05\,\mathrm{s}$ we see a relatively slower loss rate; at this point most of the atoms have been absorbed so the repulsive inter-atomic interactions, and hence the quantum pressure are weaker.

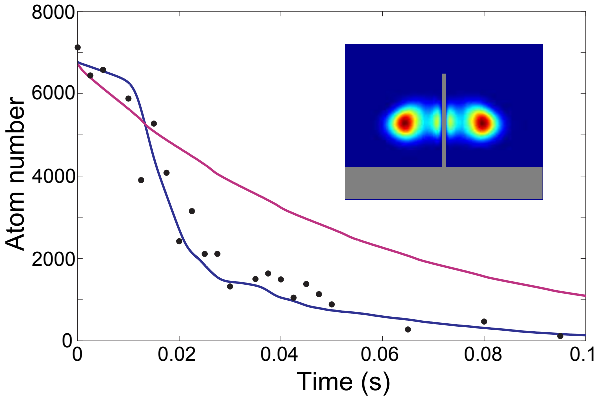

FIG. 3: BEC losses due to a nanotube, atom number plotted against time. Black points are experimental data, blue curve is for the GPE simulation with interactions, magenta curve is for a non-interacting wavepacket. Inset show the cross-section of the BEC's density profile after 0.03 seconds. Gray shapes sketch the relative position of the tube and the chip surface.

For comparison, we also show a simulation with no inter-atomic interactions [Fig 3, magenta curve]. All other parameters remain the same. We see a classic exponential decay, with a loss rate that is significantly slower than in the experiment. This reveals that the interactions are important, since they increase the quantum pressure of the wavefunction on the tube. We note that the very simple model for the CP potential is sufficient to describe the experimental data.

Up until now we have assumed the nanotube may be treated as a static object. However, it is possible that the interaction between atoms and nanotubes is significantly affected by thermal or mechanical oscillations of the nanotube. This might produce deleterious effects but conversely, might prove useful in cooling nanoscaled objects. We therefore end our investigation by considering the effects of a vibrating nanotube on a BEC. This time we consider a full three-dimensional system with the potential further simplified to a step function. The dynamics are again modeled by the Gross-Pitaevskii equation with 10^4 ^{87}Rb atoms, trap frequencies as before. The simulation begins with the BEC ground state in the trap and the tube potential is ramped up over 1 ms which simulates insertion of the tube. The tube is then oscillated sinusoidally for 0.02 s with an amplitude of $A = 1.5\,\mu\mathrm{m}$, variable frequency, f. This may be achieved by driving the tube with a piezo element. Spatial and energy cutoffs absorb atoms that are excited to very high energies by the process; we typically lose 80-90% of the atoms. The tube potential is then suddenly turned off and the one-particle density matrix of the cloud is then evaluated after averaging over 0.04 seconds. This reveals the relative occupation of the ground state mode, f_c, after Penrose-Onsager [29].

We plot f_c against the vibration frequency of the tube

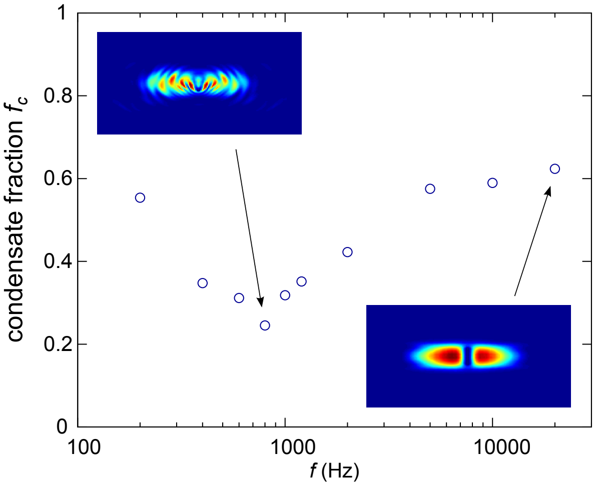

FIG. 4: Remaining condensate fraction against nanotube oscillation frequency following a 0.02s overlap. Insets show cross-section cloud profiles at the end of the oscillation process.

in Fig. 4. The insertion and removal of the tube reduces f_c to about 0.6. We see that at low frequencies this is largely maintained. However, at higher frequencies, the tube oscillations reduce f_c to around 0.2. At even higher frequencies, f_c returns to a relatively constant 0.6 (the complex dynamics lead to small fluctuations in the extracted value).

This behavior is explained by the BEC's speed of sound, v_s, and correlation time, $t_c = l_H/v_s$ where l_H is the condensate's healing length. Topological excitations and reduction of f_c first set in when the speed of the tube is greater than the local speed of sound, $A \cdot 2\pi f \gtrsim v_s$. This corresponds to $f \gtrsim 60\,\mathrm{Hz}$ in this case and the population of excited modes increases with the frequency. However, if the tube oscillates with a frequency $f \gg 1/t_c$, the gas cannot respond to the oscillations and merely sees a static, smeared potential; the disruption is minimal, and f_c is retained [Fig. 4, inset bottom right]. In our case, $1/t_c \sim 3000\,\mathrm{Hz}$, assuming the peak atom density. Between these limits, the BEC is strongly disrupted [Fig. 4, inset top left].

Nanotubes typically have a fundamental frequency $\sim 100\,\mathrm{kHz}$. We therefore conclude that natural vibrations of nanotubes are unlikely to disrupt the BEC, in spite of the high energy of the oscillations. Furthermore, undriven thermal fluctuations for typical nanotubes have an amplitude $< 5\,\mathrm{nm}$ [30]. This implies the tube would not move faster than the speed of sound in the BEC and very little disruption would occur.

In conclusion, we have studied quantum reflection from nanotubes and shown it becomes significant for Bose-Einstein condensates. We saw that the nanotube potential extracted from recent experiments was significantly weaker than that expected for metallic tubes or even a good insulator. This might be explained by surface roughness effects [25, 28]. Pairwise theories are only guaranteed to become accurate in the limit of rarified media but we find a close match with the Lifshitz theory in the dielectric case; this could potentially make design of nanodevices much simpler.

We then simulated BEC atom losses to a nanotube, finding highly non-trivial dynamics. A detailed description of the wavepacket, including quantum pressure and inter-atomic interactions was necessary to describe the experimental data. However, only very simple theories of the potential were required. Interestingly, no other loss channel, other than Casimir-Polder physics, was required to explain the results. Finally we considered how an oscillating nanotube excites a BEC. We found there is a resonance where the condensate fraction is significantly reduced at a frequency $< 1/t_c$. Very high and very low frequencies damage the condensate much less.

We gratefully acknowledge support from the DFG through SFB/TRR21, the Baden-Württemberg RiSC Programme and Kompetenznetz “Functional Nanostructures”, the Carl Zeiss Stiftung, and BW-grid computing resources.

---

[1] J. Fortágh and C. Zimmermann, Rev. Mod. Phys. **79**, 235 (2007).
[2] S. Camerer, M. Korppi, A. Jöckel, D. Hunger, T. W. Hänsch, and P. Treutlein, Phys. Rev. Lett. **107**, 223001 (2011).
[3] C. Stehle, H. Bender, C. Zimmermann, D. Kern, M. Fleischer, and S. Slama, Nat. Photon. **5**, 494 (2011).
[4] C. Zipkes, S. Palzer, C. Sias, and M. Köhl, Nature **464**, 388 (2010).
[5] S. Schmid, A. Härter, and J. H. Denschlag, Phys. Rev. Lett. **105**, 133202 (2010).
[6] B. Kasch, H. Hattermann, D. Cano, T. E. Judd, S. Scheel, C. Zimmermann, R. Kleiner, D. Koelle, and J. Fortágh, New J. Phys. **12**, 065024 (2010).
[7] D. E. Chang, C. A. Regal, S. B. Papp, D. J. Wilson, J. Yeb, O. Painter, H. J. Kimble, and P. Zoller, PNAS **107**, 1005 (2010).
[8] B. Murphy and L. V. Hau, Phys. Rev. Lett. **102**, 033003 (2009).
[9] R. Salem, Y. Japha, J. Chabé, B. Hadad, M. Keil, K. A. Milton, and R. Folman, New J. Phys. **12**, 023039 (2010).
[10] M. Gierling, P. Schneeweiss, G. Visanescu, P. Federsel, M. Haffner, D. P. Kern, T. E. Judd, A. Günther, and J. Fortágh, Nat. Nano. **6**, 446 (2011).
[11] P. Schneeweiss *et al.*, Nat. Nano., accepted (2012).
[12] M. Fink, A. Naranjo, F. Arnecke, J. Eiglsperger, H. Friedrich, J. Madroñero, P. Raab, and A. Wirzba, Phys. Rev. A **81**, 062714 (2010).
[13] Y. S. Barash and A. A. Kyasov, Sov. Phys. JETP **68**, 39 (1989).
[14] E. V. Blagov, G. L. Klimchitskaya, and V. M. Mostepanenko, Phys. Rev. B **75**, 235413 (2007).
[15] M. Boustimi, J. Baudon, P. Candori, and J. Robert,

Phys. Rev. B **65**, 155402 (2002).

[16] C. Eberlein and R. Zietal, Phys. Rev. A **80**, 012504 (2009).

[17] M. Fink, J. Eiglsperger, H. Friedrich, and J. Madroñero, Eur. Phys. J. D **63**, 33 (2011).

[18] R. F. Rajter, R. Podgornik, V. A. Parsegian, R. H. French, and W. Y. Ching, Phys. Rev. B **76**, 045417 (2007).

[19] V. A. Parsegian, *Van Der Waals Forces: A Handbook for Biologists, Chemists, Engineers, and Physicists* (Cambridge, 2006).

[20] I. V. Bondarev and P. Lambin, Phys. Rev. B **72**, 035451 (2005).

[21] R. Fermani, S. Scheel, and P. L. Knight, Phys. Rev. A **75**, 062905 (2007).

[22] M. Ashino, A. Schwarz, T. Behnke, and R. Wiesendanger, Phys. Rev. Lett. **93**, 136101 (2004).

[23] M. S. Safronova, C. J. Williams, and C. W. Clark, Phys. Rev. A **69**, 022509 (2004).

[24] L.-W. Li, M.-S. Leong, T.-S. Yeo, and P.-S. Kooi, J. Electromagn. Waves Appl. **14**, 961 (2000).

[25] S. L. Cornish, N. G. Parker, A. M. Martin, T. E. Judd, R. G. Scott, T. M. Fromhold, and C. S. Adams, Physica D **238**, 1299 (2009).

[26] F. Shimizu, Phys. Rev. Lett. **86**, 987 (2001).

[27] T. E. Judd, R. G. Scott, G. Sinuco, T. W. A. Montgomery, A. M. Martin, P. Krüger, and T. M. Fromhold, New J. Phys. **12**, 063033 (2010).

[28] T. A. Pasquini, M. Saba, G.-B. Jo, Y. Shin, W. Ketterle, D. E. Pritchard, T. A. Savas, and N. Mulders, Phys. Rev. Lett. **97**, 093201 (2006).

[29] O. Penrose and L. Onsager, Phys. Rev. **104**, 576 (1956).

[30] A. Krishnan, E. Dujardin, T. W. Ebbesen, P. N. Yianilos, and M. M. J. Treacy, Phys. Rev. B **58**, 14013 (1998).